



**HAL**  
open science

## Diamond/ $\gamma$ -alumina band offset determination by XPS

J. Cañas, G. Alba, D. Leinen, F. Lloret, M. Gutierrez, D. Eon, Julien Pernot,  
E. Gheeraert, D. Araujo

► **To cite this version:**

J. Cañas, G. Alba, D. Leinen, F. Lloret, M. Gutierrez, et al.. Diamond/ $\gamma$ -alumina band offset determination by XPS. Applied Surface Science, 2021, 535, pp.146301. 10.1016/j.apsusc.2020.146301 . hal-03167438

**HAL Id: hal-03167438**

**<https://hal.science/hal-03167438>**

Submitted on 24 Oct 2022

**HAL** is a multi-disciplinary open access archive for the deposit and dissemination of scientific research documents, whether they are published or not. The documents may come from teaching and research institutions in France or abroad, or from public or private research centers.

L'archive ouverte pluridisciplinaire **HAL**, est destinée au dépôt et à la diffusion de documents scientifiques de niveau recherche, publiés ou non, émanant des établissements d'enseignement et de recherche français ou étrangers, des laboratoires publics ou privés.



Distributed under a Creative Commons Attribution - NonCommercial 4.0 International License

# Diamond/ $\gamma$ -alumina band offset determination by XPS

J. Cañas<sup>1,2</sup>, G. Alba<sup>1</sup>, D. Leinen<sup>3</sup>, F. Lloret<sup>4</sup>, M. Gutierrez<sup>1</sup>, D. Eon<sup>2</sup>, J. Pernot<sup>2</sup>, E. Gheeraert<sup>2</sup>, D. Araujo<sup>1</sup>

<sup>1</sup> Dpto. Ciencia de los Materiales, Facultad de Ciencias, Universidad de Cádiz, 11510 Puerto Real (Cádiz), Spain

<sup>2</sup> Universite Grenoble Alpes, Institut NEEL, F-38042 Grenoble, France

<sup>3</sup> Laboratorio de Materiales y Superficie, Departamento de Física Aplicada I, Universidad de Málaga, E-29071, Málaga, Spain

<sup>4</sup> IMOMECE, IMEC vzw, 3590 Diepenbeek, Belgium

## ABSTRACT

$\gamma$ -alumina is a promising candidate for fabricating the gate of the diamond metal oxide semiconductor field effect transistor based on oxygen termination due to its high bandgap of 6.7 eV and high static dielectric constant of 9. Besides these properties, having a sufficient barrier for holes is mandatory to avoid carriers leakage through the gate. However, the band offset of the diamond/alumina heterojunction can be affected by the alumina crystallinity and interface bonds, which depend on multiple factors such as deposition and annealing temperature or diamond surface treatment prior to deposition.

In this work, the heterojunction of atomic layer deposited alumina and (100) p-diamond is studied using X-ray photoelectron spectroscopy (XPS). Transmission electron microscopy studies reveal that the deposited alumina layer is 35 nm thick and present the gamma phase. The valence band offset between diamond and  $\gamma$ -alumina is evaluated on a single sample with a new methodology based on an ion etching XPS depth profile. The obtained value for the valence band offset of diamond and  $\gamma$ -alumina is 3.4 eV.

## 1. Introduction

Diamond is expected to become the cornerstone of future power devices due to its superior properties: Wide band gap of 5.5 eV, high breakdown field, high carrier mobility and high thermal conductivity [1]. The research made in diamond growth during the last decade has started to bear fruits, allowing the fabrication of diamond metal oxide field effect transistors (MOSFET). Most of them have been fabricated using the surface 2D hole gas channel produced in hydrogen terminated diamond [2–5]. This 2D gas is understood as transfer doping between diamond valence band (VB) electrons and surface adsorbents energy levels below diamond valence band [6,7]. Remarkably, this 2D hole gas can also exist in a diamond/oxide interface despite the absence of adsorbents [8]. This is tentatively explained by the argument that a high dipole in the interface would allow electrons from diamond valence band to be transferred to some lower energy defect level in the oxide near the interface. However, the proximity of the transferred electrons and the 2D hole gas dramatically reduces the carrier's mobility of the 2D hole gas due to ionic scattering reducing the performance of the H-Diamond MOSFET [9,10].

Another alternative is to fabricate a diamond MOSFET using oxygen terminated diamond, whose surface displays an insulator behaviour [11]. By using a low-doped oxygen terminated diamond, bulk carrier concentration can be controlled by field effect using a metal oxide semiconductor (MOS) capacitor structure. This allows having a channel with high concentration of majority carriers and high mobility, working in MOS accumulation regime; and alternatively, the full depletion of the majority carriers working in deep depletion regime [12-15]. However, a relatively high density of interface states ( $>10^{12} \text{ cm}^{-2} \text{ eV}^{-1}$ ) and parasitic leakage currents, that reduce the electrical performance of the diamond MOS, are usually observed.

In order to have a proper interface, atomic layer deposition (ALD) is used to grow gate oxides thin films as it is reported to give rise to low ( $10^{11} \text{ cm}^{-2} \text{ eV}^{-1}$ ) interface states due to its surface limiting nature [16].  $\gamma$ -alumina grown by ALD is a great candidate to fabricate the gate of the oxygen terminated diamond MOSFET due to its high bandgap of 6.8 eV [17], high dielectric constant of 9 and thermal stability up to more than 1000°C [18-19]. However, the properties of the alumina are extremely dependent on the synthesis process. The temperature of the ALD is a fundamental factor in order to archive a surface limiting process to grow the oxide layer by layer. Also, the interface chemistry of the first ALD cycles is crucial since the terminations of diamond react only partially with the ALD precursors. Another important factor is the thickness of the alumina layer, as it is known to influence the crystalline phase of the oxide affecting the displayed electrical properties. The influence of the thickness on the microstructure arises from various fundamental factors for these thin films: a) the stress produced by the mismatch of the lattices, b) the lack of material that hinder crystallization and c) the surface nucleation process. Specifically, ALD grown alumina over oxygen terminated diamond is known to be amorphous for very thin films ( $< 10 \text{ nm}$ ) even deposited at 380°C. For the same ALD conditions, films above 20 nm were shown to be polycrystalline with low angle grain boundaries [20].

These different phases do not only have different bulk properties, but also, the interface charge distribution can be severely affected by the interface atomic structure for the heterovalent junction

between alumina and diamond producing changes in the band offset. The valence band offset (VBO) between diamond and alumina depends on two terms: i) The coulombic chemical potential of both materials, which is a pure bulk property. ii) The interface dipolar term, which is the difference between the averaged electrostatic potential energies across the interface. The bulk term is sensitive to the crystallographic structure of the alumina. The interface term is dependent on both, the symmetry of the interface (i.e. crystalline phase of the oxide) and the interfacial bonds, as the charge transfer between donor-like and acceptor-like bonds is largely responsible for VBO variation at heterovalent interfaces [21].

Previous studies on both O- and H- terminated diamond/amorphous alumina interface have been carried out with X-ray photoelectron spectroscopy (XPS)[22–24]. In these works, the VBO has been calculated using three different samples: Pure alumina and diamond samples and a thin ~2 nm film of amorphous alumina deposited over a diamond substrate to study the interface between both materials. This method avoids XPS charging effects and allow the measurement of the VBO by referencing diamond and alumina VB to a specific core level. However, to study diamond/ $\gamma$ -alumina interface by XPS, a thicker layer must be deposited in order to synthetize the  $\gamma$  phase. According to our knowledge, no systematic studies for ALD grown crystalline  $\gamma$  –alumina/diamond interface chemistry have been reported up to now although similar studies have been reported for  $\gamma$  –alumina/SiC interface [25].

In this work,  $\gamma$ -alumina grown by ALD on to p- (100) diamond has been studied by XPS. Low energy ion beam bombardment XPS depth profile has been performed through the alumina layer and the interface with diamond. The recorded XPS spectra have been used to study the VBO of the diamond/ $\gamma$ -alumina junction using a unique sample, taking into account crystallographic effects and post-ALD interface chemistry.

## 1. Experimental procedure

The sample is an O-terminated (100)-oriented p-diamond covered with a thin layer of ALD alumina. For its fabrication, first a boron-doped diamond film was grown by chemical vapour deposition on to a (100)-oriented high-temperature high-pressure diamond substrate in a Nyrim type reactor. The boron concentration of this film is estimated as a few  $10^{17} \text{ cm}^{-3}$ . After diamond growth, the resultant surface was exposed to an ozone treatment produced by deep UV light. The substrate was inserted into a chamber with 500 mbar of oxygen-gas. Then, the UV lamp was turned on and ozone was produced for 2h. After, it

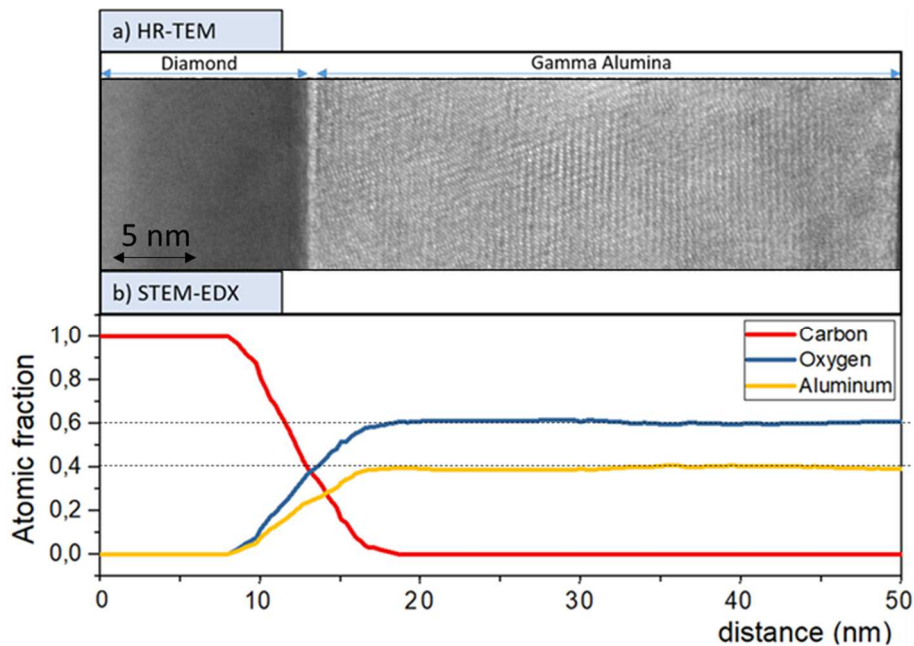


**Fig. 1:** a) High resolution transmission electron microscopy (HRTEM) image of the interface between p-(100) diamond and ALD alumina. The alumina layer presents 35 nm of polycrystalline  $\gamma$ -alumina. b) STEM-EDX Atomic fraction profile through the alumina layer and its interface with diamond. The stoichiometry of the alumina shows a constant near 40:60 ratio of Al/O all over the 35 nm film.

was submitted to a 400 cycles ALD process for the alumina deposition in a Savannah 100 deposition system from Cambridge NanoTech. For this purpose, a chamber temperature of 380 °C was used. The precursor used was trimethylaluminum (TMA) and the oxidant was H<sub>2</sub>O. TMA and water were consecutively injected in the chamber in short pulses of 0.015 s and purged with N<sub>2</sub> after 5 s in between. The alumina layer was submitted after to an annealing treatment at 1000°C in high vacuum (10<sup>-6</sup> mbar) for 1 hour with 6 hours heating ramp and 6 hours cooling ramp in order to acquire a crystalline alumina layer.

The resultant alumina layer was studied by high resolution transmission electron microscopy (HRTEM) and by scanning transmission electron microscopy in energy dispersive spectroscopy (STEM-EDS) mode. Concerning the lamella preparation, the sample was nano-machined with Ga<sup>+</sup> in a Helios Nanolab 650 SEM-FIB. The lamella was characterized with a FEI-THALOS electron microscope at 300 keV. HRTEM studies reveal that the layer is 35 nm thick. Its crystalline structure corresponds to an fcc crystal, therefore, it is attributed to the  $\gamma$ -alumina as reported in previous contribution[20]. STEM-EDS compositional profile through the interface shows a stoichiometry of near 40% Al / 60% O for the whole alumina layer. These results are shown in **Fig. 1**.

Concerning the XPS study, all the measurements were carried out using a high resolution monochromatic Al-K $\alpha$  radiation ( $h\nu=1486.6$  eV) with a PHI 5700 equipment. The spectra were recorded using a 0.1 eV step and a 23.5 eV pass energy. The peak contributions were extracted by combining a Lorentzian and a Gaussian function (Voigt profile). The background was subtracted using Tougaard background model function [26]. XPS depth profile was performed through the alumina layer with low energy (0.5 kV) and oblique angle (57°) Ar<sup>+</sup> sputtering, while applying a Zalar compucentric rotation normal to the surface. A scheme of the etching process is represented in **Fig. 2a**. XPS measurements have been performed alternately (to the sputtering) in the wells as it is represented in **Fig. 2b**. The alternated XPS measurement and sputtering were stopped when the whole XPS signal was attributed to diamond. The XPS depth profile spectra have been used to determine the  $\gamma$ -alumina stoichiometry and bandgap and to study the VBO of the diamond/ $\gamma$ -alumina interface using only one sample, taking into account crystallographic effects and post-ALD interface chemistry. The determination of the VBO is performed by taking a reference core level from the alumina spectrum from which the interfacial spectrum is fixed. The alumina valence band maximum (VBM) is determined in the pure alumina spectrum and the diamond VBM is directly determined in the interface spectrum. The VBO is determined from the difference between diamond and  $\gamma$ -alumina VBMs as both spectra are well referenced to the Al(2p) core level at the interface. With this methodology, the alumina bandgap, stoichiometry and the VBO have been consistently determined.

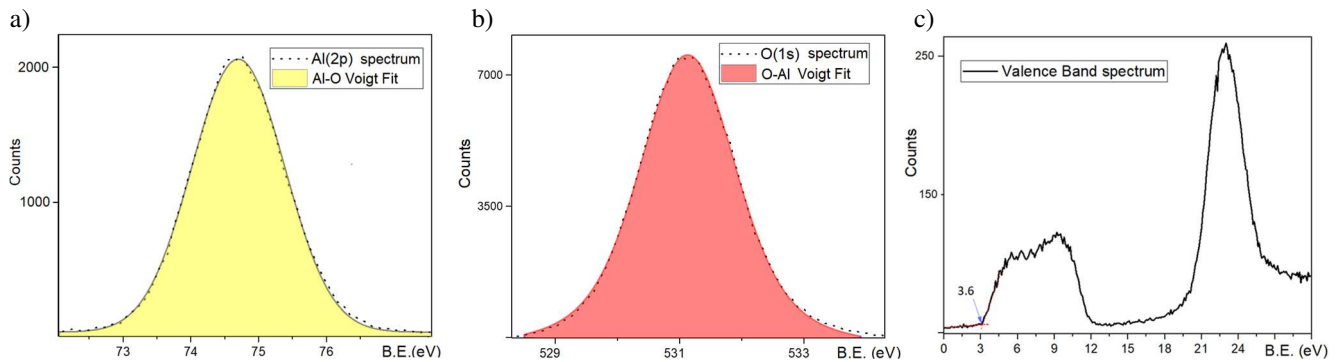


**Fig. 3:** XPS spectra from measurement (i) on top of the  $\gamma$ -alumina layer. a) Background subtracted Al(2p) peak. The whole contribution is assigned to an Al-O bond. b) Background subtracted O(1s) peak. The whole contribution is assigned to an O-Al bond. c) Valence band spectrum from alumina. The VBM is assigned as the first point coming out from the background at 3.6 eV. The peak at 23 eV corresponds to the O(2s) spectrum.

## 2. Results and discussion

### 2.1. $\gamma$ -alumina analysis

A first XPS measurement, here after referred to as measurement (i), is performed on top of the alumina layer after a mild  $\text{Ar}^+$  cleaning. Since the inelastic mean free path of a photoelectron ejected from the alumina at  $\sim 1$  keV is of  $\sim 2.5$  nm [27], all the signal is unambiguously attributed to alumina. In the **Fig. 3**, the XPS core levels and VB spectra from the measurement (i) are represented. **Fig. 3a** shows the Al (2p) spectrum centred at 74.6 eV after the subtraction of the background. The energy position of the XPS core levels is sensitive to the chemical environment due to the different charge shielding of the outer electrons involved in bonding. As expected, the whole Al (2p) area is attributed to aluminium bonded to oxygen (Al-O) as there is no contribution for metallic aluminium at lower energies in the spectrum. In the **Fig. 3b**, the O (1s) spectrum centred at 531.3 eV is shown. Analogously, the whole area of this peak is attributed to oxygen bonded to aluminium atoms (O-Al). By using the relative sensitive factor (RSF) provided by the manufacturer of the XPS equipment, the relation between oxygen and aluminium core levels provides a stoichiometry for the alumina layer of 37.9% for aluminium and 42.1% for oxygen. In

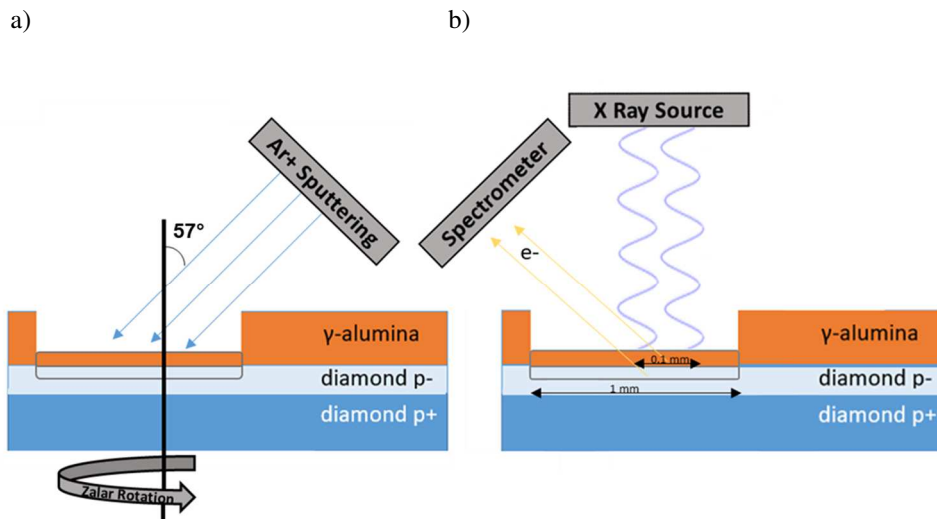


**Fig. 2** a) Schematic representation of the sputter etching process of the alumina layer. The sample has been sputtered using 0.5 kV  $\text{Ar}^+$  ions at  $33^\circ$  incidence angle with respect to the sample surface while Zalar compucentric sample rotation was performed. Sputtering was carried out in-situ in the spectrometer to alternately record XPS spectra and etch the alumina layer until reaching its interface with the diamond substrate.

b) Scheme of the XPS measurement in which the X rays are focussed vertically downwards onto a 0.1 mm diameter spot inside the 1 mm diameter sputter crater. Photoelectrons were recorded at a take-off angle of  $45^\circ$ .

the **Fig. 3c**, the alumina VB is represented. The first two peaks at 6 eV and 9 eV are associated with  $\gamma$ -alumina VB and the bigger peak at 23 eV is attributed to the O(2s) level. The VBM has been determined using the linear fit method [22–24], in **Fig. 3c** the VBM is estimated as 3.6 eV. The energy values of the peaks maximums from measurement (**i**) are summarized in **Table 1**.

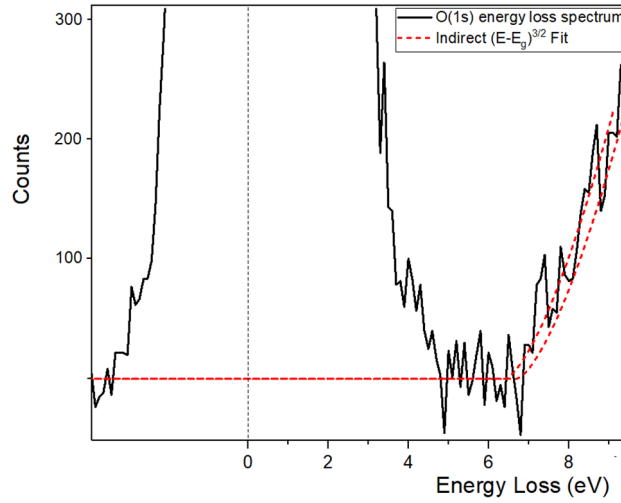


**Fig. 4:** O(1s) photoelectron energy loss spectrum (PEELS) centred at the O(1s) maximum. An indirect  $(E-E_g)^{3/2}$  bandgap loss function is used to fit the energy loss feature yielding a bandgap value of  $6.7 \pm 0.2$  eV.

Additionally, **Fig. 4** shows the alumina O(1s) spectrum from the measurement (**i**) without the background subtraction and with its peak maximum energy value set as zero. In the ideal case, photoexcited electrons from this core level will be collected with a kinetic energy  $K.E. = h\nu - B.E. - \phi$ , where B.E. is the electron binding energy and  $\phi$  the work function of the spectrometer. However, some of them can interact with other electrons suffering inelastic scattering energy losses before leaving the material. These inelastic losses are related to collective excitation or band transitions. Therefore, at higher B.E. (lower K.E.) in the O(1s) spectrum these bandgap-related transitions can be observed. This phenomenon allows us to study the energy loss spectroscopy of the ejected photoelectrons and measure the bandgap of the compound. However, the fraction of inelastic scattered ejected photoelectrons will be of the order of 1%. Thus, in order to have enough signal to clearly distinguish the energy loss features, the energy loss spectrum must be studied using a core peak with a high cross section, to provide enough signal, as in the case of O(1s) spectrum. These inter band and plasmon losses result in a characteristic signal at higher B.E. in which the intensity is proportional to a  $(E-E_{gap})^n$  curve. For indirect transitions that are dependent on the momentum transferred by the incident photoelectron to the crystal electrons, the product of the indirect matrix element and the density of states yields a  $(E-E_{gap})^{3/2}$  term for the spectrum. A detailed description of this phenomenon was given by Rafferty and Brown [28]. The ‘zero’ of the indirect  $(E-E_{gap})^{3/2}$  fitted curve to the photoelectron energy loss spectrum is the measured bandgap. An indirect curve fit yields a value of  $6.7 \pm 0.2$  eV for the  $\gamma$ -alumina bandgap. This value is in good correspondence with previous reported values and suggest that no  $Ar^+$  sputtering related defects that can narrow the alumina bandgap are present in the layer [17,29].

## 2.2. Valence band offset determination

In previous works [22-24,30], the VBO between alumina and diamond is calculated using Kraut’s method by means of the following expression:

$$VB_{offset} = (C(1s)_{C-C} - VBM)_{diamond} - (Al(2p)_{Al-O} - VBM)_{alumina} - (C(1s)_{C-C} - Al(2p)_{Al-O})_{interface} \quad (1)$$

Where  $C(1s)_{C-C}$  represents the  $sp^3$  C-C peak position inside the deconvolved C(1s) spectrum,  $Al(2p)_{Al-O}$  represents the alumina contribution peak position inside the deconvolved Al(2p) spectrum. The first term corresponds to a spectrum recorded from a first pure diamond sample, the second recorded from a second pure alumina sample and the third recorded from the interface between diamond/alumina in a third

sample, where both materials core peaks are distinguished in the spectrum. However, the reported methodology to calculate the VBO is imprecise for diamond/ $\gamma$ -alumina interface because the alumina is amorphous in the third sample, as thin (<10 nm) films are not crystalline[20], and because carbon surface contamination C(1s) is easily misunderstood with diamond C(1s) core level. Moreover, energy levels associated with diamond surface chemical termination that are present in diamond VB spectrum in the first sample are not necessarily conserved in the growth process of the oxide film. In fact, if the oxide is deposited with ALD, surface reactions between ALD precursors and surface species might alter the VB of the diamond. This is highly probable in O-terminated diamond as the TMA is expected to react with surface hydroxyl groups.

In this work, the interface between diamond and  $\gamma$ -alumina is studied in a unique sample by means of a XPS depth profile performed through the alumina layer with low energy (0.5 kV) and oblique angle ( $57^\circ$ ) Ar<sup>+</sup> sputtering. Performed SRIM [31] simulations conclude that irradiating the alumina with Ar<sup>+</sup>, at this oblique angle and low energy, introduce the implantation peak well before the first two nanometers. As the XPS signal comes from the first ~8 nm due to the combined inelastic mean free path of the electrons escaping from the diamond/alumina interface, the chemical properties of the interface can be studied guaranteeing that the main part of our signal is coming from the non-implanted crystalline alumina, interface and diamond [31-33].

The VBO can be directly measured using only two terms in the same sample taking into account post-ALD interface chemistry and preserving the crystallography of the alumina film. This method can be summarized in the following Eq (3):

$$VB_{offset} = (Al(2p)_{Al-O} - VBM_{diamond})_{interface} - (Al(2p)_{Al-O} - VBM)_{alumina} \quad (2)$$

Spectra number	0.5 kV Ar <sup>+</sup> sputter time [min]	Al2p			O1s			C1s			VBM [eV]	$\gamma$ -Al <sub>2</sub> O <sub>3</sub> /diamond [at%]
		FWHM [eV]	BE [eV]	Atomic Concentration [%]	FWHM [eV]	BE [eV]	Atomic Concentration [%]	FWHM [eV]	BE [eV]	Atomic Concentration [%]		
i)	2	1.5	<b>74.6</b>	37.2	1.9	531.3	62.0	-	~284.4	0.8	3.6	100%
ii)	30	1.6	<b>74.6</b>	37.3	1.8	531.3	61.4	-	~284.4	1.27	3.7	$\gamma$ -Al <sub>2</sub> O <sub>3</sub>
iii)	80	1.7	<b>74.6</b>	20.2	2.0	531.4	34.2	1.8	284.0	46.6	0.3	63/47
iv)	82	2.0	<b>74.6</b>	11.8	2.0	531.4	19.9	1.9	284.1	69.3	0.3	42/68
v)	95	-	~74.4	-	-	~530.9	-	1.77	<b>284.1</b>	98.3	0.2	100% diamond

**Table 1:** The binding energy values of the peaks maximums (BE), the full with at half maximum (FWHM), the atomic concentration and the valence band maximum (VBM) for the five XPS measurements at different depths are presented. The estimated errors in FWHM, BE and VBM are 0.1 eV.

The first term is the energy difference measured between the  $Al(2p)_{Al-O}$  of the alumina to the VBM of the diamond at the XPS spectrum recorded interface. This can be measured because diamond VB does not overlap the alumina VB near the VBM region at the interface as their VBO is sufficiently high. This way the interface bonds associated energy levels and their charge distribution effects are present in the spectrum. The second term is the energy difference between the  $Al(2p)_{Al-O}$  to the alumina VBM of the XPS spectrum recorded at the pure alumina. As the  $Al(2p)$  spectrum remains unaffected at the interface because aluminium atoms are not bonded to carbon atoms,  $Al(2p)$  provides an excellent reference point to fix both diamond and aluminium VB at the interface spectrum.

The XPS measurements at different depth are plotted in the **Fig. 5**, and their peaks maximum energies, FWHM and VBM are displayed in the **Table 1**. The measurements **(i)** (after 2 mins of  $Ar^+$  sputtering) and **(ii)** (after 30 mins of  $Ar^+$  sputtering) in **Fig. 5** are characteristic of alumina. The  $Al(2p)$  at 74.6 eV was used as reference for centring these two pure alumina spectra. The detailed analysis of the measurement **(i)** was presented in last section. In fact, both spectra are in perfect correspondence in terms of VB,  $Al(2p)$  and  $O(1s)$  shapes, areas and their corresponding distances. The VBM of the measurement **(ii)** has been determined to be 3.7 eV, again making use of the linear fit method. After 30 min  $Ar^+$  sputtering the stoichiometry of the layer remains 37.7% aluminium and 62.3% oxygen.

The measurements **(iii)** (after 80 mins of  $Ar^+$  sputtering) and **(iv)** (after 82 mins of  $Ar^+$  sputtering) are representative from the alumina/diamond interface as they have both contributions from  $Al(2p)$  and  $C(1s)$ . Both spectra are fixed again thanks to the  $Al(2p)$ , as there is no chemical shift due to an Al-C bonding contribution from the interface. This is compatible with our knowledge from the ALD process interface chemistry between TMA and O-terminated diamond. In the VB spectrum range for these two measurements, the diamond VB contribution is superimposed to the alumina VB contribution, however, the VB of diamond is distinguished at lower energies. The VBM of diamond has been determined using the linear fit method on the lower energy range of the VB. A VBM value of 0.3 eV is obtained for measurement **(iii)** and for measurement **(iv)**. The stoichiometry extracted from measurement **(iii)** and **(iv)** is the same: 37.2% of aluminium and 62.8% of oxygen. Therefore, no sign of preferential sputtering is

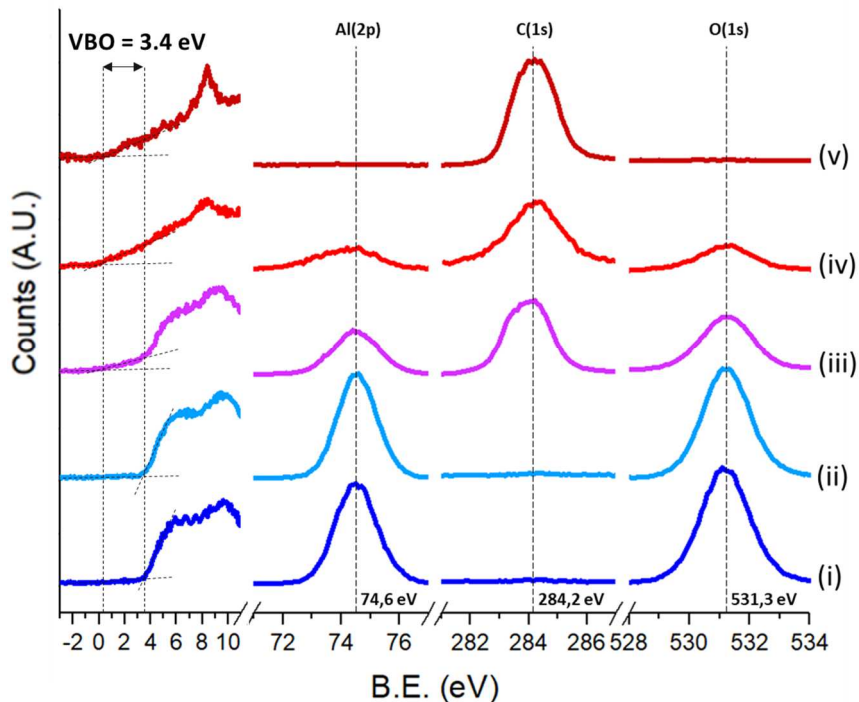


**Fig. 5:**  $Ar^+$  sputtering depth profile XPS spectra. Represented curves heights are not representative, some of them have been scaled for the better comprehension of the graph. The spectra of the VBs and representative core levels for the five XPS measurements performed alternately to the  $Ar^+$  etching are represented. The measurements **(i)** and **(ii)** are characteristic of the alumina. The measurements **(iii)** and **(iv)** are characteristic of the interface. The measurement **(v)** is characteristic of the diamond substrate reached after the  $Ar^+$  etching has removed the whole alumina layer. A VBO of 3.4 eV is deduced from the VBM differences by direct application of Eq. (2), as the value of the  $Al(2p)$  maximum has been used as a reference for centring the spectra of every measurement (except for measurement **(v)** which is fixed to have  $C(1s)$  maximum in the same position as measurements **(iii)** and **(iv)**).

found as the stoichiometry of the layer remain constant through the whole etching process.

The XPS measurement (v) is a pure diamond spectrum as no contribution of alumina is observed. The centre of the C(1s) is fixed at 284.2 eV to be aligned with the interfacial measurements (iii) and (iv). A VBM value of 0.2 eV is obtained from measurement (v). It is in good concordance with the interfacial spectra and with previously reported diamond VB even though low Ar<sup>+</sup> implantation might have occurred in diamond. The distance C(1s)-VBM is 283.9 eV, which is in the range of values reported in literature [33].

Finally, taking the values of this section, the VBO between  $\gamma$ -alumina and (100)-oriented p-doped diamond can be calculated with Eq. (1) or Eq. (2). This is performed in Table 2 with different combinations of the obtained spectra. The VBO can be also deduced from Fig. 5 as it the graphical representation of Eq. (2). The VBO between diamond and  $\gamma$ -alumina is  $3.4 \pm 0.2$  eV.

Spectra used in formula (1)	v), i), iii)	v), ii), iii),	v), i),iv)	v), ii),iv)	Spectra used in formula (2)	iii),i)	iv),i)	iii),ii)	iv),ii)
VBO	3.5 eV	3.6 eV	3.4 eV	3.5 eV	VBO	3.3 eV	3.3 eV	3.4 eV	3.4 eV

**Table 2:** Diamond/ $\gamma$ -alumina VBO calculated using different spectra and formulas (1) and (2). The binding energy of the representative core levels (BE) and the valence band maximum (VBM) values for the different combinations of XPS measurements presented in Table 1 are introduced in formula (1) and (2) in order to calculate the band offset. The average value is  $3.4 \pm 0.2$  eV.

### 2.3. Band setting and discussion

The VBO between  $\gamma$ -alumina and (100)-oriented p-doped oxygen terminated diamond is  $3.4 \pm 0.2$  eV, as discussed in the previous section. Therefore, a staggered band setting with a conduction band offset (CBO) of  $2.2 \pm 0.4$  eV is deduced using diamond and  $\gamma$ -alumina bandgap values. These results together with the interface chemistry are summarized in Fig. 6.

The VBO reported here is higher than the value previously reported between alumina and diamond using XPS, where many of the values are in the range of 1-2 eV [22–24]. One of the reasons that explain the large difference in the VBO is the particularly low value for the C(1s)-VBM distance found in these studies: 282.3 eV in (100) oriented O-terminated [22], 282.2 eV in p type (111) oriented H-terminated diamond [23] and 283.1 eV in (111) oriented H terminated diamond [24]. These values are far away from values reported by Kono et al. [33] in his detailed revision of diamond XPS studies in which the C(1s)-VBM distance is in the range of 283.9 eV to 284.4 eV, compatible with the value reported here (283.9 eV). A higher value of the C(1s)-VBM distance leads to a higher VBO, thus explaining the difference between this work and the previously reported values for the VBO. However, the XPS studies submitted by Yang et al. [34] reporting that the VBO of O<sub>2</sub> plasma enhanced ALD alumina over H-diamond is 2.7 eV, Marechal et al. [23] reporting a value for the VBO of 2.7 on (111) oriented H-diamond and Ren et al. [35] reporting a value of 3.3 eV for the VBO in H-terminated diamond are values close to the one reported here. Additionally, synchrotron radiation photoemission and XANES measurements on NO<sub>2</sub>-exposed H-terminated diamond and alumina found a VBO of 3.9 eV [36].

In the present work, the high value of the VBO could be attributed to the modification of the interfacial dipole related to the reconfiguration of the interface due to the crystallization of the alumina. The crystallization of the alumina leads to a redistribution of interface charges affecting the interface dipole and producing a higher value of VBO to those measured for O-diamond and amorphous alumina. Moreover, the latter XPS works need to use three different samples, which can also introduce some uncertainty of the VBO estimation. In contrast, the methodology used in this work removes surface contamination and provides a method to determine the VBO in a single sample where the Al(2p) peak is used to fix the different XPS spectra consistent with the interface chemistry and microstructure.

In conclusion, the resulting band setting shows a great potential barrier for holes while there is no barrier for electrons flowing from diamond to  $\gamma$ -alumina. This implies that  $\gamma$ -alumina is not the definitive material in terms of band setting for fabricating a diamond p-MOS as the inversion regime cannot be reached due to the absence of barrier for electrons. However, in terms of band setting,  $\gamma$ -alumina is suitable for reaching both accumulation and depletion regimes. This is of special interest in new developed diamond transistors architectures such as deep depletion diamond MOSFET[15] in which diamond never reach inversion but deep depletion regime due to the immense minority carrier generation time.

### 3. Conclusions

An accurate methodology to measure the VBO between two materials by XPS that requires a single sample has been presented. Applying this methodology, the band offset for a (100)-oriented oxygen terminated p-doped diamond substrate and a 35 nm polycrystalline  $\gamma$ -alumina layer has been measured taking into account oxide crystallographic effects and post oxide deposition interface chemistry. After measuring a bandgap of  $6.7 \pm 0.2$  eV using the energy loss of the O(1s), the diamond/  $\gamma$ -alumina VBO is reported to be  $3.4 \pm 0.2$  eV and the CBO  $2.2 \pm 0.4$  eV. Such results make very attractive ALD grown alumina as oxide gate for some architectures of diamond MOSFET where no inversion regime is required.

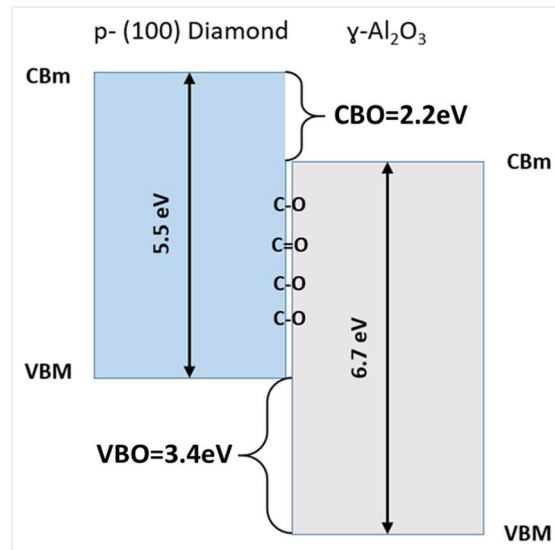


**Fig. 6:** Band setting and interface chemistry scheme between  $\gamma$ -alumina and p- (100)-oriented diamond.

---

#### 4. Acknowledgement:

We thank the Ministerio de Economía y Competitividad (MINECO) of the Spanish Government for funding under Grants No. TEC2017-86347-C2-1-R (DiamMOS project) and No. ESP2017-91820-EXP (Diam-Air, EXPLORA project) from FEDER funds. We thank to EU Framework Programme for research & Innovation – H2020 for funding under Grant No. SEP-210184415 (GreenDiamond project) of (H2020-LCE-20141.640947 program).

---

#### 5. References

- [1] K. Thonke, The boron acceptor in diamond, *Semicond. Sci. Technol.* 18 (2003). <https://doi.org/10.1088/0268-1242/18/3/303>.
- [2] J. Liu et al., An Overview of High-k Oxides on Hydrogenated-Diamond for Metal-Oxide-Semiconductor Capacitors and Field-Effect Transistors, *Sensors*. 813 (2018) 1–17. <https://doi.org/10.3390/s18060813>.
- [3] J.W. Liu, M.Y. Liao, M. Imura, H. Oosato, E. Watanabe, Y. Koide, Electrical characteristics of hydrogen-terminated diamond metal-oxide-semiconductor with atomic layer deposited HfO<sub>2</sub> as gate dielectric, *Appl. Phys. Lett.* 102 (2013) 2–6. <https://doi.org/10.1063/1.4798289>.
- [4] H. Kawarada, H. Tsuboi, T. Naruo, T. Yamada, D. Xu, A. Daicho, T. Saito, A. Hiraiwa, C-H surface diamond field effect transistors for high temperature (400 °C) and high voltage (500 V) operation, *Appl. Phys. Lett.* 105 (2014) 013510. <https://doi.org/10.1063/1.4884828>.
- [5] S. Kono, T. Teraji, D. Takeuchi, M. Ogura, H. Kodama, A. Sawabe, Direct determination of the barrier height of Au ohmic-contact on a hydrogen-terminated diamond (001) surface, *Diam. Relat. Mater.* 73 (2017) 182–189. <https://doi.org/10.1016/j.diamond.2016.09.015>.
- [6] W. Chen, D. Qi, X. Gao, A.T.S. Wee, Surface transfer doping of semiconductors, *Prog. Surf. Sci.* 84 (2009) 279–321. <https://doi.org/10.1016/j.progsurf.2009.06.002>.
- [7] M.T. Edmonds, M. Wanke, A. Tadich, H.M. Vulling, K.J. Rietwyk, P.L. Sharp, C.B. Stark, Y. Smets, A. Schenk, Q.H. Wu, L. Ley, C.I. Pakes, Surface transfer doping of hydrogen-terminated diamond by C60F48: Energy level scheme and doping efficiency, *J. Chem. Phys.* 136 (2012) 1–10. <https://doi.org/10.1063/1.3695643>.
- [8] M. Tordjman, K. Weinfeld, R. Kalish, Boosting surface charge-transfer doping efficiency and robustness of diamond with WO<sub>3</sub> and ReO<sub>3</sub>, *Appl. Phys. Lett.* 111 (2017). <https://doi.org/10.1063/1.4986339>.
- [9] C.E. Nebel, C. Sauerer, F. Ertl, M. Stutzmann, C.F.O. Graeff, P. Bergonzo, O.A. Williams, R. Jackman, Hydrogen-induced transport properties of holes in diamond surface layers, *Appl. Phys. Lett.* 79 (2001) 4541–4543. <https://doi.org/10.1063/1.1429756>.
- [10] C. Nebel, Surface transfer-doping of H-terminated diamond with adsorbates, *New Diam. Front. Carbon Technol.* 15 (2005) 2005. <http://www.myu-inc.jp/myukk/NDFCT/archives/pdf/NDFCT492.pdf>.
- [11] M. Tachiki, Y. Kaibara, Y. Sumikawa, M. Shigeno, H. Kanazawa, T. Banno, K.S. Song, H. Umezawa, H. Kawarada, Characterization of locally modified diamond surface using Kelvin probe force microscope, *Surf. Sci.* 581 (2005) 207–212. <https://doi.org/10.1016/j.susc.2005.02.054>.
- [12] G. Chicot, A. Maréchal, R. Motte, P. Muret, E. Gheeraert, J. Pernot, Metal oxide semiconductor structure using oxygen-terminated diamond, *Appl. Phys. Lett.* 102 (2013). <https://doi.org/10.1063/1.4811668>.
- [13] P. Muret, D. Eon, E. Gheeraert, N. Rouger, Comprehensive electrical analysis of metal / Al<sub>2</sub>O<sub>3</sub> / O-terminated diamond capacitance Comprehensive electrical analysis of metal / Al<sub>2</sub>O<sub>3</sub> / O-terminated diamond capacitance, *Journal of Applied Physics* 123, 161523 (2018);
- [14] T. Matsumoto, H. Kato, K. Oyama, T. Makino, M. Ogura, D. Takeuchi, T. Inokuma, N. Tokuda, S. Yamasaki, Inversion channel diamond metal-oxide-semiconductor field-effect transistor with normally off characteristics., *Sci. Rep.* 6 (2016) 31585. <https://doi.org/10.1038/srep31585>.
- [15] T.T. Pham, N. Rouger, C. Masante, G. Chicot, F. Udreá, D. Eon, E. Gheeraert, J. Pernot, Deep depletion concept for diamond MOSFET, *Appl. Phys. Lett.* 111 (2017). <https://doi.org/10.1063/1.4997975>.
- [16] S.M. George, Atomic Layer Deposition : An Overview, (2010) 111–131.
- [17] J. Cañas, J.C. Piñero, F. Lloret, M. Gutierrez, T. Pham, J. Pernot, D. Araujo, Determination of alumina bandgap and dielectric functions of diamond MOS by STEM-VEELS, *Appl. Surf. Sci.* 461 (2018) 93–97. <https://doi.org/10.1016/j.apsusc.2018.06.163>.
- [18] J. Musil, J. Blažek, P. Zeman, Š. Prokšová, M. Šašek, R. Čerstvý, Thermal stability of alumina

- thin films containing  $\gamma$ -Al<sub>2</sub>O<sub>3</sub> phase prepared by reactive magnetron sputtering, *Appl. Surf. Sci.* 257 (2010) 1058–1062. <https://doi.org/10.1016/j.apsusc.2010.07.107>.
- [19] I. Levin, D. Brandon, Metastable Alumina Polymorphs: Crystal Structures and Transition Sequences, *J. Am. Ceram. Soc.* 81 (2005) 1995–2012. <https://doi.org/10.1111/j.1151-2916.1998.tb02581.x>.
- [20] M. Gutiérrez, F. Lloret, T. Pham, J. Cañas, D. Reyes, D. Eon, J. Pernot, D. Araújo, Control of the Alumina Microstructure to Reduce Gate Leaks in Diamond MOSFETs, *Nanomaterials.* 8 (2018) 584. <https://doi.org/10.3390/nano8080584>.
- [21] R.T. Tung, L. Kronik, Charge Density and Band Offsets at Heterovalent Semiconductor Interfaces, 1700001 (2018) 1–15. <https://doi.org/10.1002/adts.201700001>.
- [22] E. A. Marechal, M.Aoukar, C. Vallée, C. Rivière, D. Eon, J. Pernot, Gheeraert, Energy-band diagram configuration of Al<sub>2</sub>O<sub>3</sub>/oxygen-terminated p-diamond metal-oxide-semiconductor, *Appl. Phys. Lett.* 107 (2015). <https://doi.org/10.1016/j.wear.2007.01.010>.
- [23] A. Maréchal, Y. Kato, M. Liao, S. Koizumi, Interfacial energy barrier height of Al<sub>2</sub>O<sub>3</sub>/H-terminated (111) diamond heterointerface investigated by X-ray photoelectron spectroscopy, *Appl. Phys. Lett.* 111 (2017) 1–6. <https://doi.org/10.1063/1.5001070>.
- [24] J.W. Liu, M.Y. Liao, M. Imura, Y. Koide, Band offsets of Al<sub>2</sub>O<sub>3</sub> and HfO<sub>2</sub> oxides deposited by atomic layer deposition technique on hydrogenated diamond, *Appl. Phys. Lett.* 101 (2012) 252108. <https://doi.org/10.1063/1.4772985>.
- [25] Zhang, G. Sun, L. Zheng, S. Liu, B. Liu, L. Dong, L. Wang, W. Zhao, X. Liu, G. Yan, L. Tian, Y. Zeng, Interfacial study and energy-band alignment of annealed Al<sub>2</sub>O<sub>3</sub> films prepared by atomic layer deposition on 4H-SiC, *J. Appl. Phys.* 113 (2013) 2–6. <https://doi.org/10.1063/1.4789380>
- [26] P. Tougaard, S.; Simund, Elastic and inelastic scattering of electrons reflected from solids: Effects on energy spectra, *Phys. Rev. B.* 25 (1982) 4452–4466. <https://doi.org/10.1103/PhysRevB.25.4452>.
- [27] H. Shinotsuka, S. Tanuma, C.J. Powell, D.R. Penn, Calculations of electron inelastic mean free paths. X. Data for 41 elemental solids over the 50eV to 200keV range with the relativistic full Penn algorithm, *Surf. Interface Anal.* 47 (2015) 871–888. <https://doi.org/10.1002/sia.5789>.
- [28] B. Rafferty, L.M. Brown, Direct and indirect transitions in the region of the band gap using electron-energy-loss spectroscopy, *Phys. Rev. B.* 58 (1998) 10326–10337. <https://doi.org/10.1103/PhysRevB.58.10326>.
- [29] Guo, H. Zheng, S.W. King, V. V. Afanas'ev, M.R. Baklanov, J.F. Demarneffe, Y. Nishi, J.L. Shohet, Defect-induced bandgap narrowing in low-k dielectrics, *Appl. Phys. Lett.* 107 (2015). <https://doi.org/10.1063/1.4929702>.
- [30] E.A. Kraut, R.W. Grant, J.R. Waldrop, S.P. Kowalczyk, Semiconductor core-level to valence-band maximum binding-energy differences: Precise determination by x-ray photoelectron spectroscopy, *Phys. Rev. B.* 28 (1983) 1965–1977. <https://doi.org/10.1103/PhysRevB.28.1965>.
- [31] J.F. Ziegler, M.D. Ziegler, J.P. Biersack, SRIM - The stopping and range of ions in matter (2010), *Nucl. Instruments Methods Phys. Res. Sect. B Beam Interact. with Mater. Atoms.* 268 (2010) 1818–1823. <https://doi.org/10.1016/j.nimb.2010.02.091>.
- [32] P. Francz, G Kania, Photoelectron Spectroscopy Study of Natural (100), (110), (111) and CVD Diamond Surfaces, *Phys. Status Solidi.* 91 (1996).
- [33] S. Kono, T. Kageura, Y. Hayashi, S.G. Ri, T. Teraji, D. Takeuchi, M. Ogura, H. Kodama, A. Sawabe, M. Inaba, A. Hiraiwa, H. Kawarada, Carbon 1s X-ray photoelectron spectra of realistic samples of hydrogen-terminated and oxygen-terminated CVD diamond (111) and (001), *Diam. Relat. Mater.* 93 (2019) 105–130. <https://doi.org/10.1016/j.diamond.2019.01.017>.
- [34] Y. Yang, F.A. Koeck, M. Dutta, X. Wang, S. Chowdhury, R.J. Nemanich, Y. Yang, F.A. Koeck, M. Dutta, X. Wang, S. Chowdhury, R.J. Nemanich, Al<sub>2</sub>O<sub>3</sub> dielectric layers on H-terminated diamond : Controlling surface conductivity Al<sub>2</sub>O<sub>3</sub> dielectric layers on H-terminated diamond : Controlling surface conductivity, 155304 (2017).
- [35] Z. Ren, D. Lv, J. Xu, J. Zhang, J. Zhang, K. Su, C. Zhang, Y. Hao, High temperature (300 °C) ALD grown Al<sub>2</sub>O<sub>3</sub> on hydrogen terminated diamond: Band offset and electrical properties of the MOSFETs, *Appl. Phys. Lett.* 116 (2020) 013503. <https://doi.org/10.1063/1.5126359>.
- [36] K. Takahashi, M. Imamura, K. Hirama, M. Kasu, Electronic states of NO<sub>2</sub>-exposed H-terminated diamond/Al<sub>2</sub>O<sub>3</sub> heterointerface studied by synchrotron radiation photoemission and X-ray absorption spectroscopy, *Appl. Phys. Lett.* 104 (2014) 072101. <https://doi.org/10.1063/1.4865929>.

